On the Design of Spline-Based Lenses for the Conformal Miniaturization of Linear Antenna Arrays

M. Salucci, G. Oliveri, N. Anselmi, and A. Massa

Abstract

This work deals with the conformal miniaturization of linear antenna arrays. Towards this end, a novel synthesis approach based on the Material-by-Design (*MbD*) paradigm is proposed. The presented methodology exploits the integration of a two-step quasi-conformal transformation optics (*QCTO*) approach with a source inversion (*SI*) strategy. One the one hand, the purpose of the *QCTO* is to synthesize a meta-material covering that is able to restore the radiation features of the radiating system once its geometry has been matched to an arbitrary conformal profile. On the other hand, the *SI* allows to reduce the number of required radiators in the final conformal geometry without introducing visible alterations to the desired radiation features. Some numerical results are shown in order to validate the proposed *MbD* synthesis approach for the design of meta-material lenses based on spline curves.

1 Spline Profile #1 - $N' = 20$

1.1 Validation vs. Lens Thickness (s)

- **Virtual & Physical Geometries**

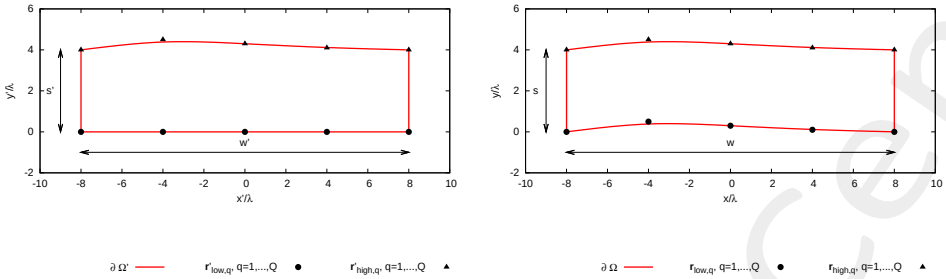

(a) (b)

Figure 1: Transformation regions and geometric parameters of interest.

- Width: $w = w' = 16.0$ $[\lambda]$;
- Lens thickness: $s = s' = \{4.0; 2.0\}$ $[\lambda]$;
- Number of spline control points: $Q = 5$;
- Control points in physical geometry:
  - $x_{low,q} \in [-w/2, w/2]$, $q = 1, ..., Q$ (equally-distributed);
  - $x_{high,q} = x_{low,q}$, $q = 1, ..., Q$;

$y_{low,1}$ $[\lambda]$	$y_{low,2}$ $[\lambda]$	$y_{low,3}$ $[\lambda]$	$y_{low,4}$ $[\lambda]$	$y_{low,5}$ $[\lambda]$
0.0	0.5	0.3	0.1	0.0

Table I: y-coordinate of the control points for the lower spline in physical space.

  - $y_{high,q} = (y_{low,q} + s)$, $q = 1, ..., Q$;
- Control points in virtual geometry:
  - $x'_{low,q} = x_{low,q}$, $q = 1, ..., Q$; $y'_{low,q} = 0.0$, $q = 1, ..., Q$;
  - $x'_{high,q} = x_{high,q}$, $q = 1, ..., Q$; $y'_{high,q} = y_{high,q}$, $q = 1, ..., Q$;

- **Virtual Array**
  - Number of elements, spacing, aperture: $N' = 20$, $d' = \frac{\lambda}{2}$, $L' = 9.5$ $[\lambda]$;
  - Distance from PEC ground plane (placed at $y' = 0.0$): $\delta' = \frac{\lambda}{4}$;
  - Excitations: $I_n = 1.0$, $\varphi_n = \frac{-2\pi}{\lambda} x_n sin(\phi_s + 90)$; $n = 1, ..., N'$;

- **QCTO**
  - Discretization cell dimension: 0.15 $[\lambda]$ (0.01 $[\lambda]$ for source mapping);

1.1.1 Results of the Transformation

Transformation Grids

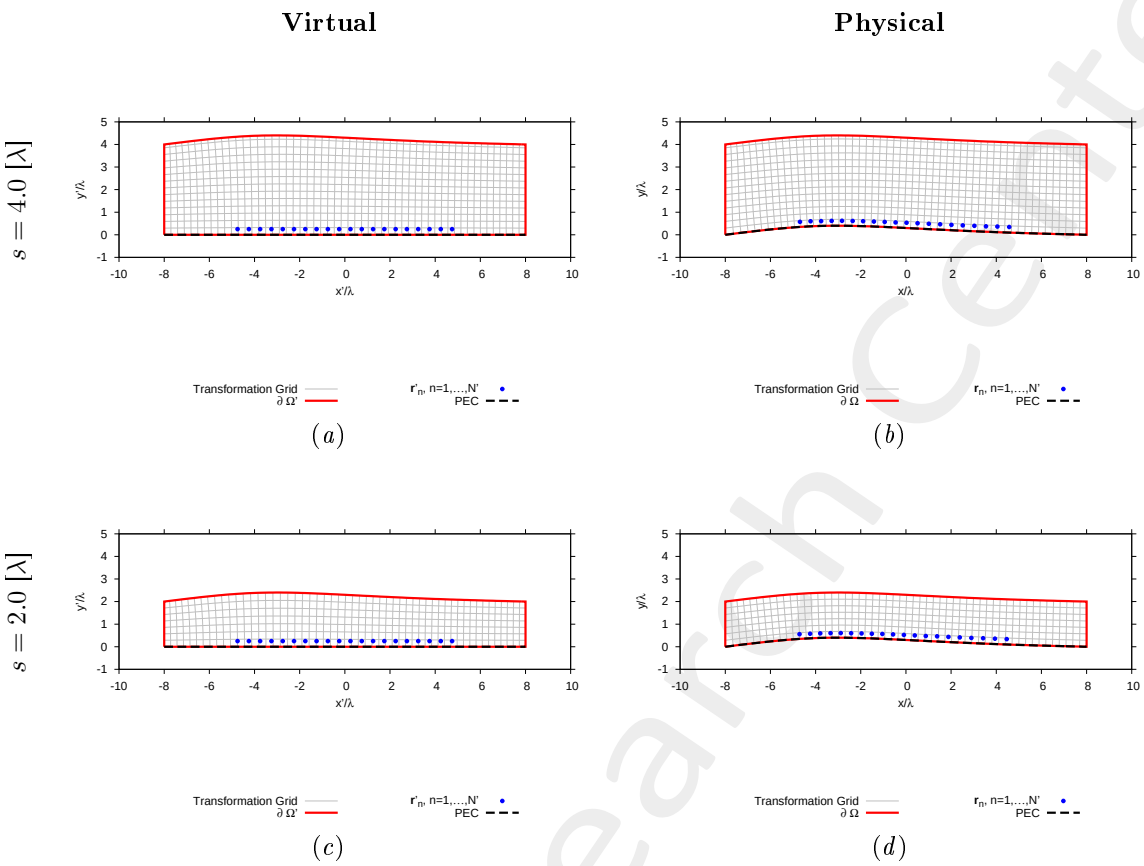

Figure 2: Transformation grids for virtual and physical geometries.

Lens Permittivity - $s = 4.0$ **[**λ**]**

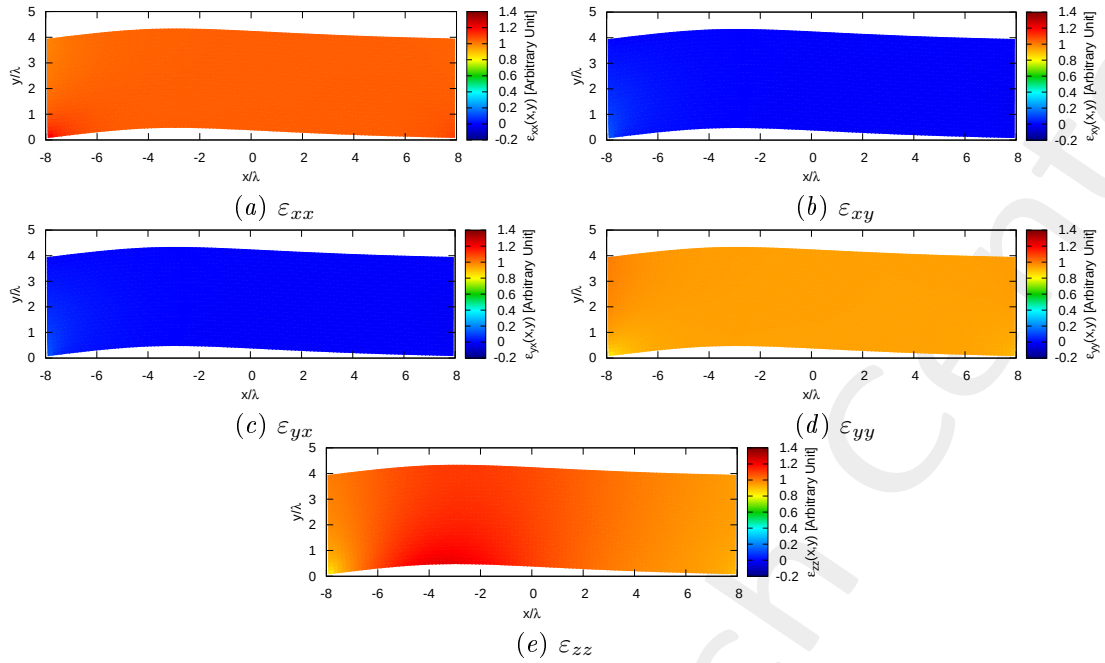

(a) ε_{xx} (b) ε_{xy}

(c) ε_{yx} (d) ε_{yy}

(e) ε_{zz}

Figure 3: Components of the relative permittivity tensor of the lens.

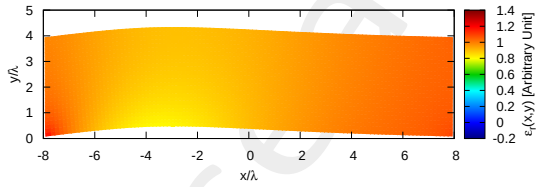

Figure 4: Isotropic approximate permittivity distribution of the lens.

Lens Permittivity - $s = 2.0$ [λ]

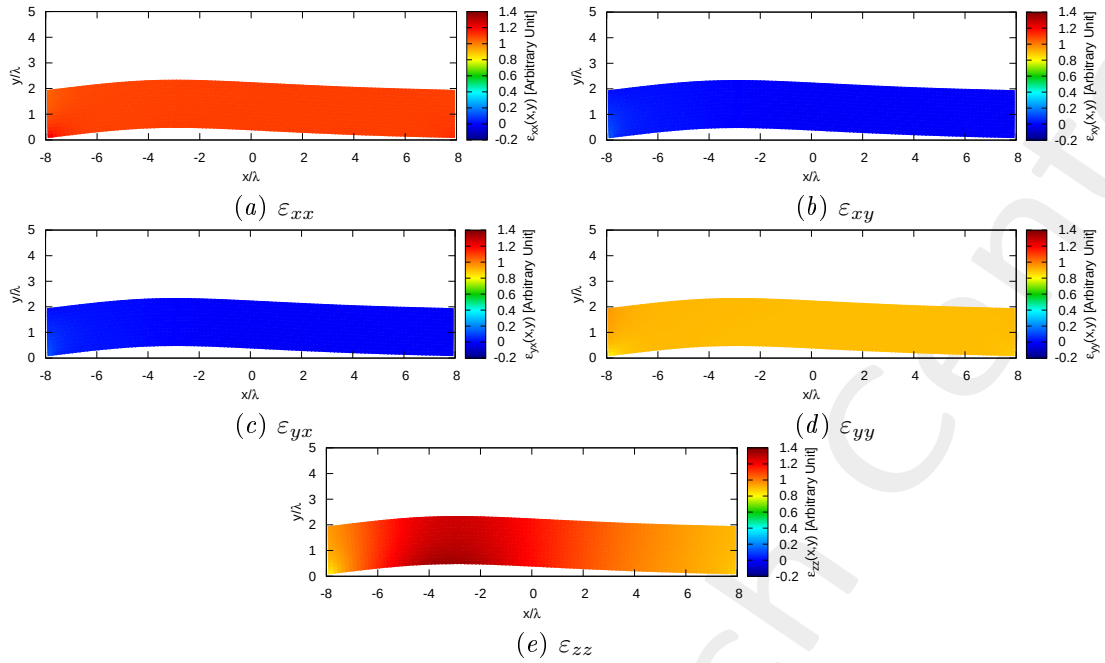

(a) ε_{xx} (b) ε_{xy} (c) ε_{yx} (d) ε_{yy} (e) ε_{zz}

Figure 5: Components of the relative permittivity tensor of the lens.

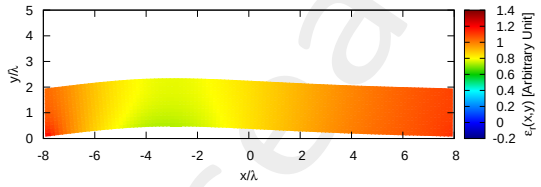

Figure 6: Isotropic approximate permittivity distribution of the lens.

Physical Lens Parameters

Lens Thickness $s = 4.0$ $[\lambda]$	
Anisotropic Permittivity Range	$[-0.02, 1.28]$
Isotropic Permittivity Range	$[0.00, 1.23]$
Lens Thickness $s = 2.0$ $[\lambda]$	
Anisotropic Permittivity Range	$[-0.02, 1.36]$
Isotropic Permittivity Range	$[0.00, 1.25]$

Table II: Permittivity ranges for the physical lens.

1.1.2 Far-Field Patterns (Aniso-Lens)

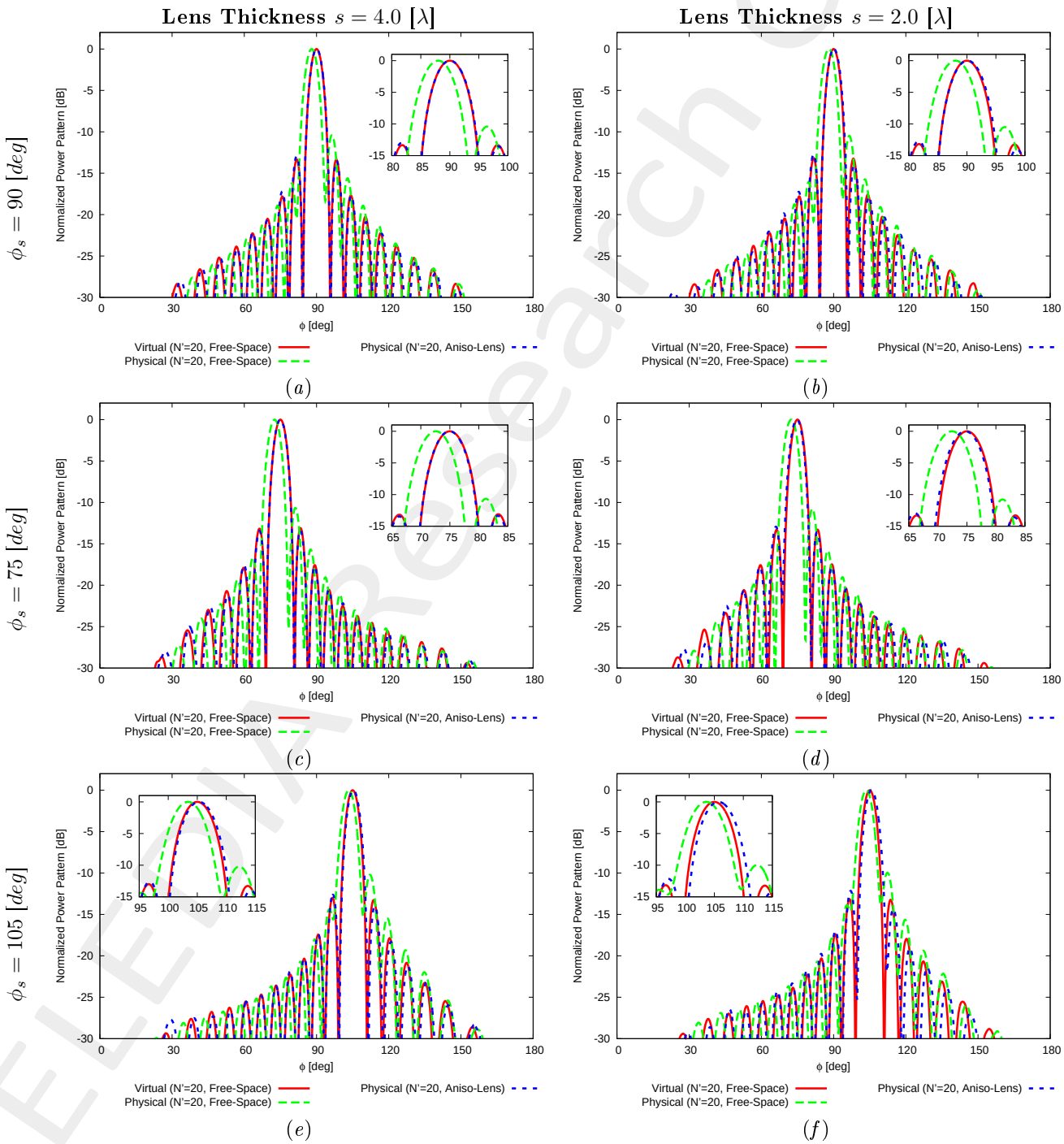

Figure 7: Comparison between the far field patterns.

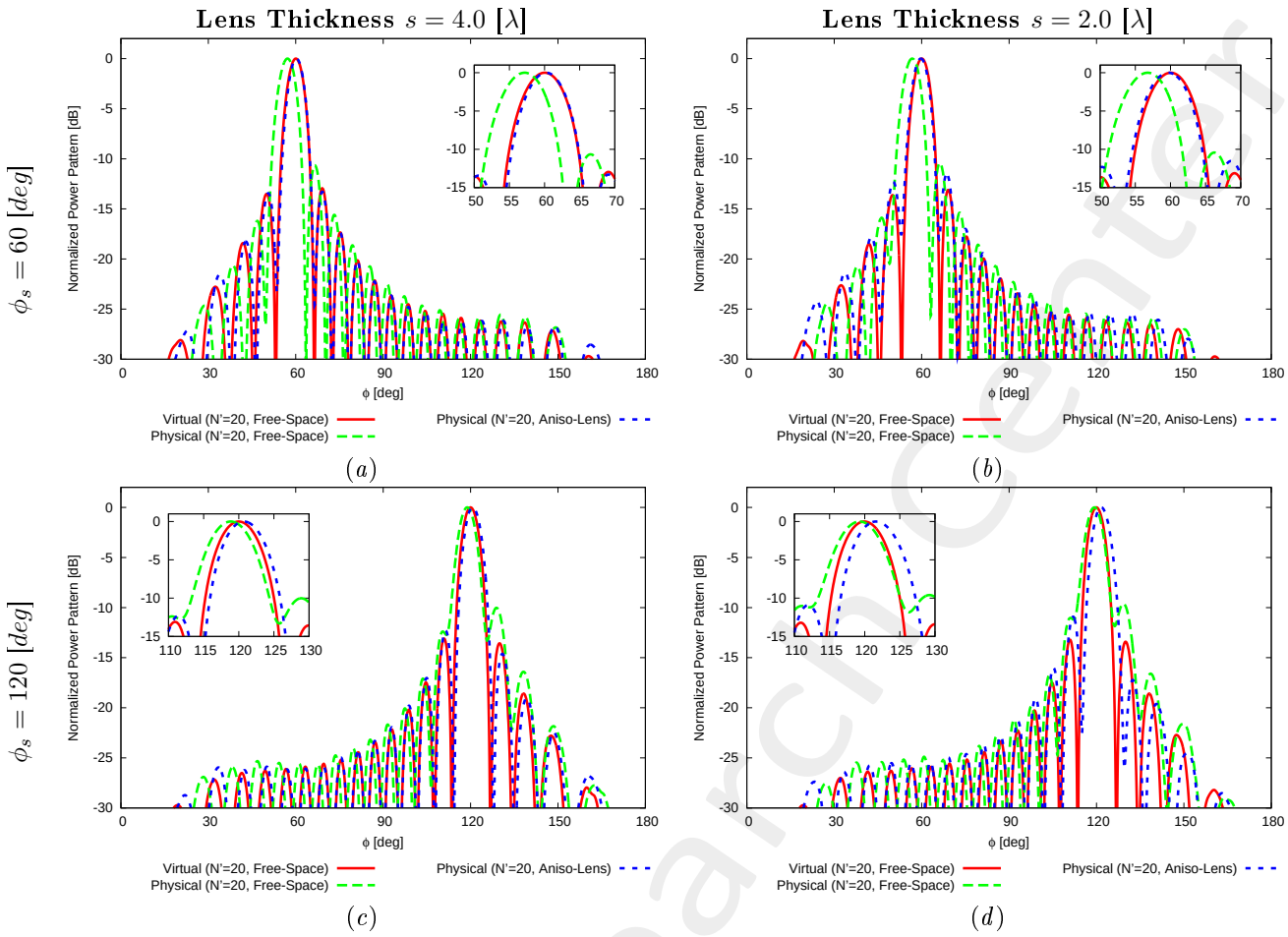

Figure 8: Comparison between the far field patterns.

1.2 Reduction of the Control Points through SI ($N' \rightarrow N < N'$)

Parameters

- Number of array elements before SI: $N' = 20$;
- Number of array elements after SI (N): check table below;
- Spacing after SI: $d = \lambda/2$;
- Radius of the observation domain: $r_{SI} = 50.0$ [λ];
- Number of field sampling points: $n_{SI} = 1000$.

	Before SI		**After SI**	
s [λ] (Lens Thickness)	N'	L [λ]	N	L [λ]
4.0	20	9.273	19	9.0
2.0	20	9.181	19	9.0

Table III: Parameters considered for SI.

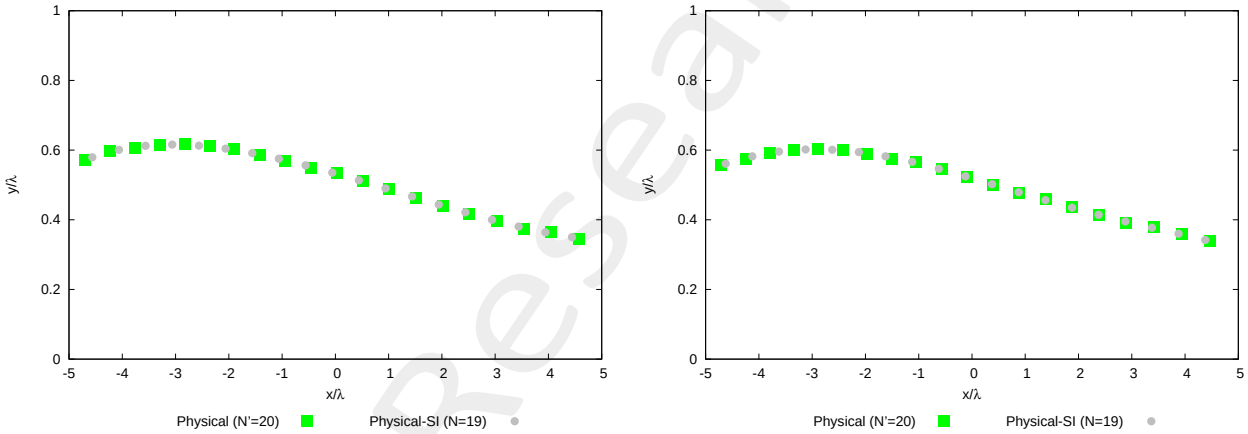

(a) $s = 4.0$ [λ] (b) $s = 2.0$ [λ]

Figure 9: Geometry of the physical array before (N') and after SI ($N < N'$).

1.2.1 Synthesized Excitations

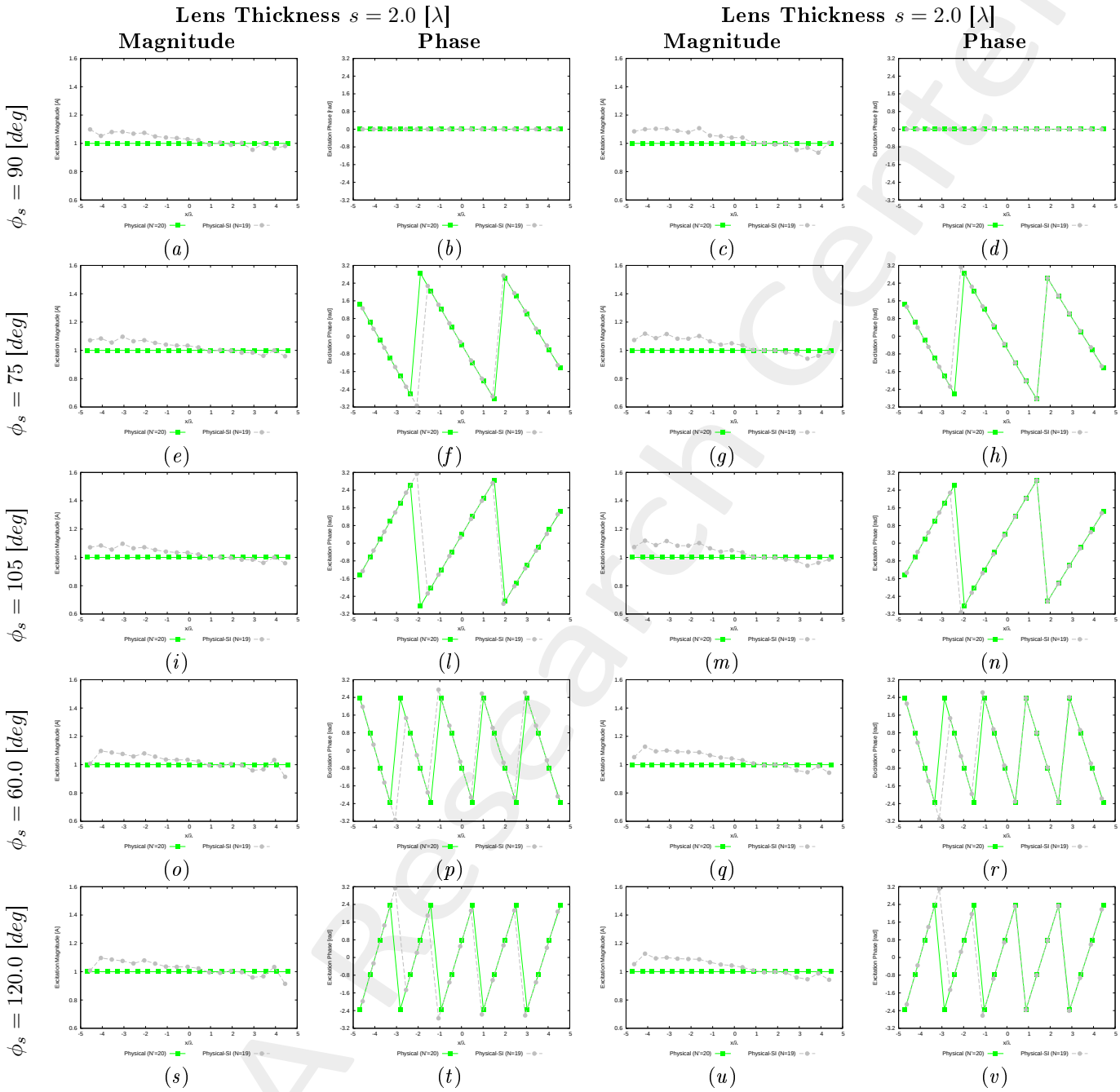

Figure 10: Magnitude and phase of the excitations of the physical array before (N') and after SI ($N < N'$).

1.2.2 Free-Space Far-Field Patterns (check SI)

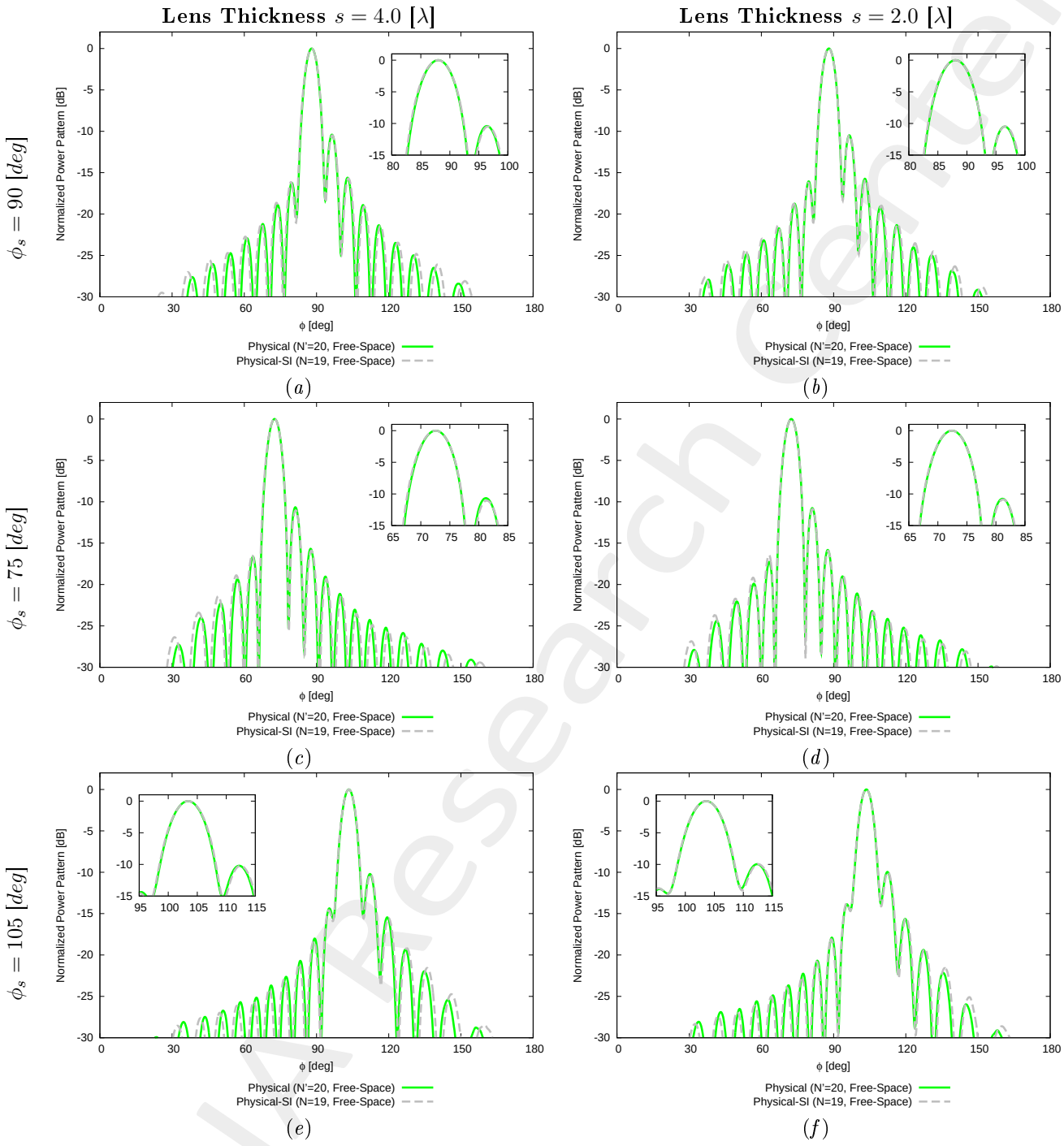

Figure 11: Free-Space patterns: Physical ($N' = 20$) vs. Physical-SI ($N < N'$).

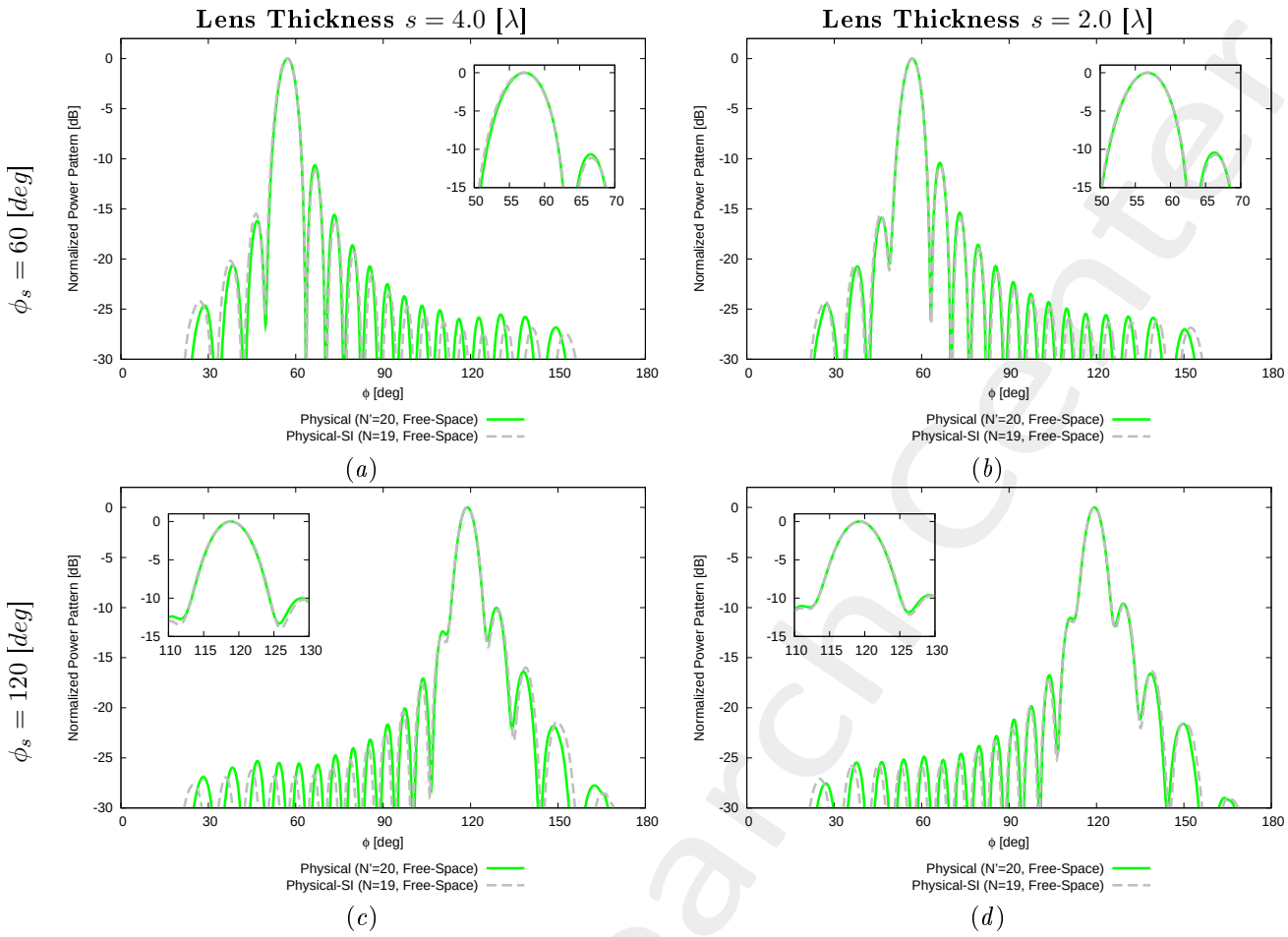

Figure 12: Comparison between the far field patterns.

Observations

- The better matching for $s = 2.0$ [λ] is due to the fact that for this case L is modified from 9.181 [λ] to 9.0 [λ], while for $s = 4.0$ [λ] the change is from 9.273 [λ] to 9.0 [λ].

1.2.3 Near-Field Distributions (Aniso-Lens, $\phi_s = 90$ [deg])

Lens Thickness $s = 4.0$ [λ]

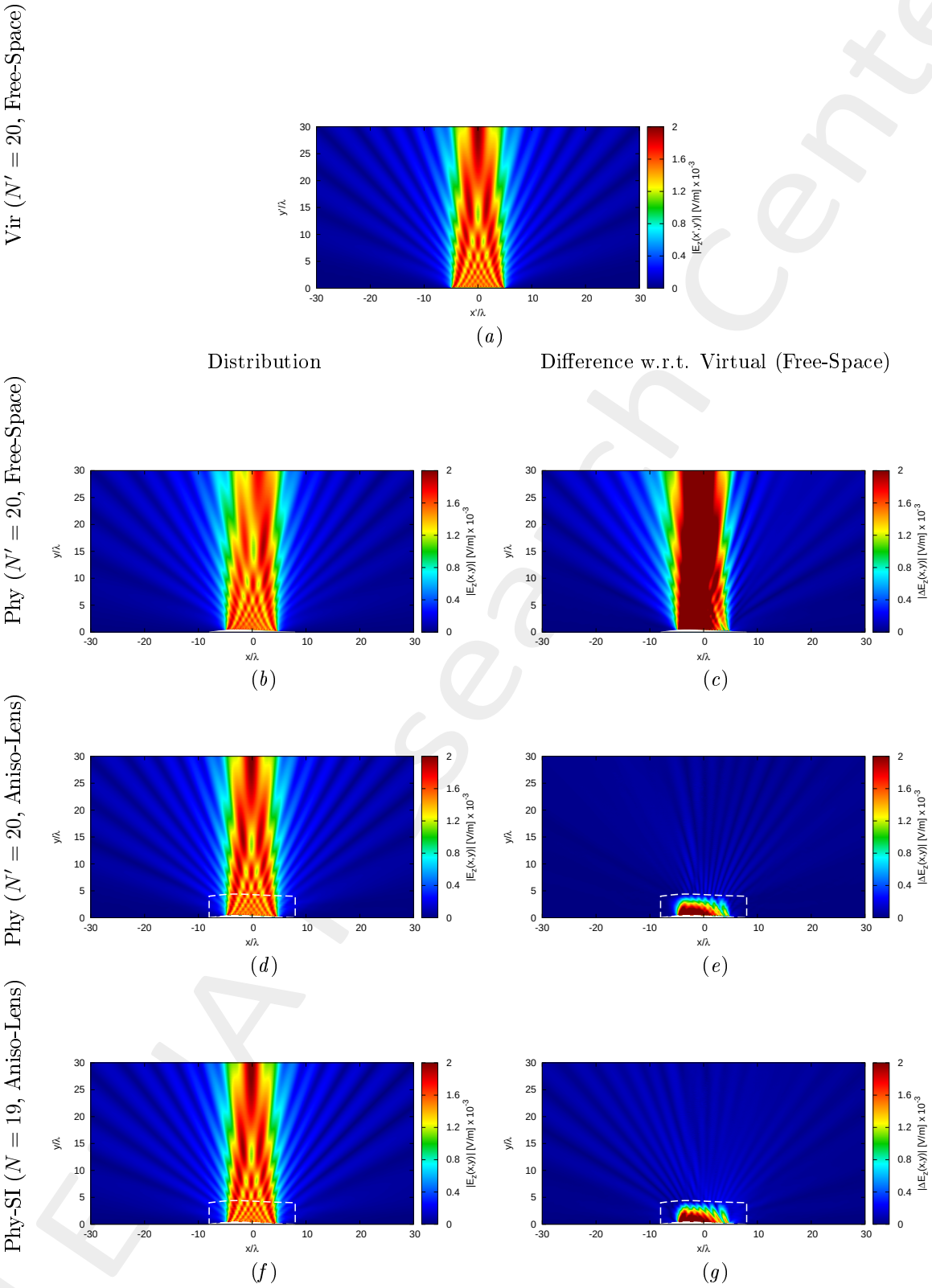

Figure 13: Lens Thickness $s = 4.0$ [λ] - Electric field distributions.

Lens Thickness $s = 2.0$ $[\lambda]$

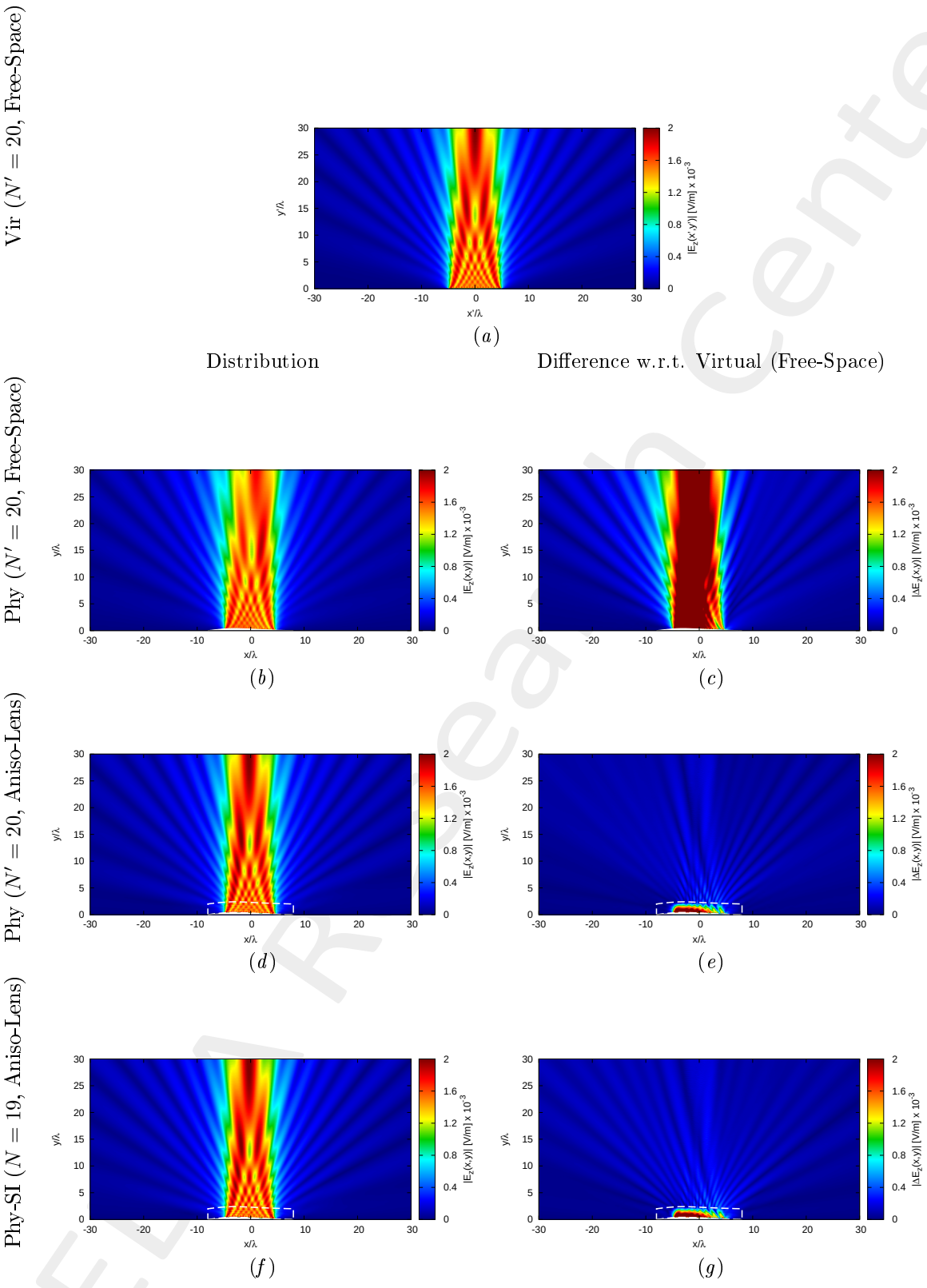

Figure 14: Lens Thickness $s = 2.0$ $[\lambda]$ - Electric field distributions.

1.2.4 Near-Field Distributions (Aniso-Lens, $\phi_s = 75$ [deg])

Lens Thickness $s = 4.0$ [λ]

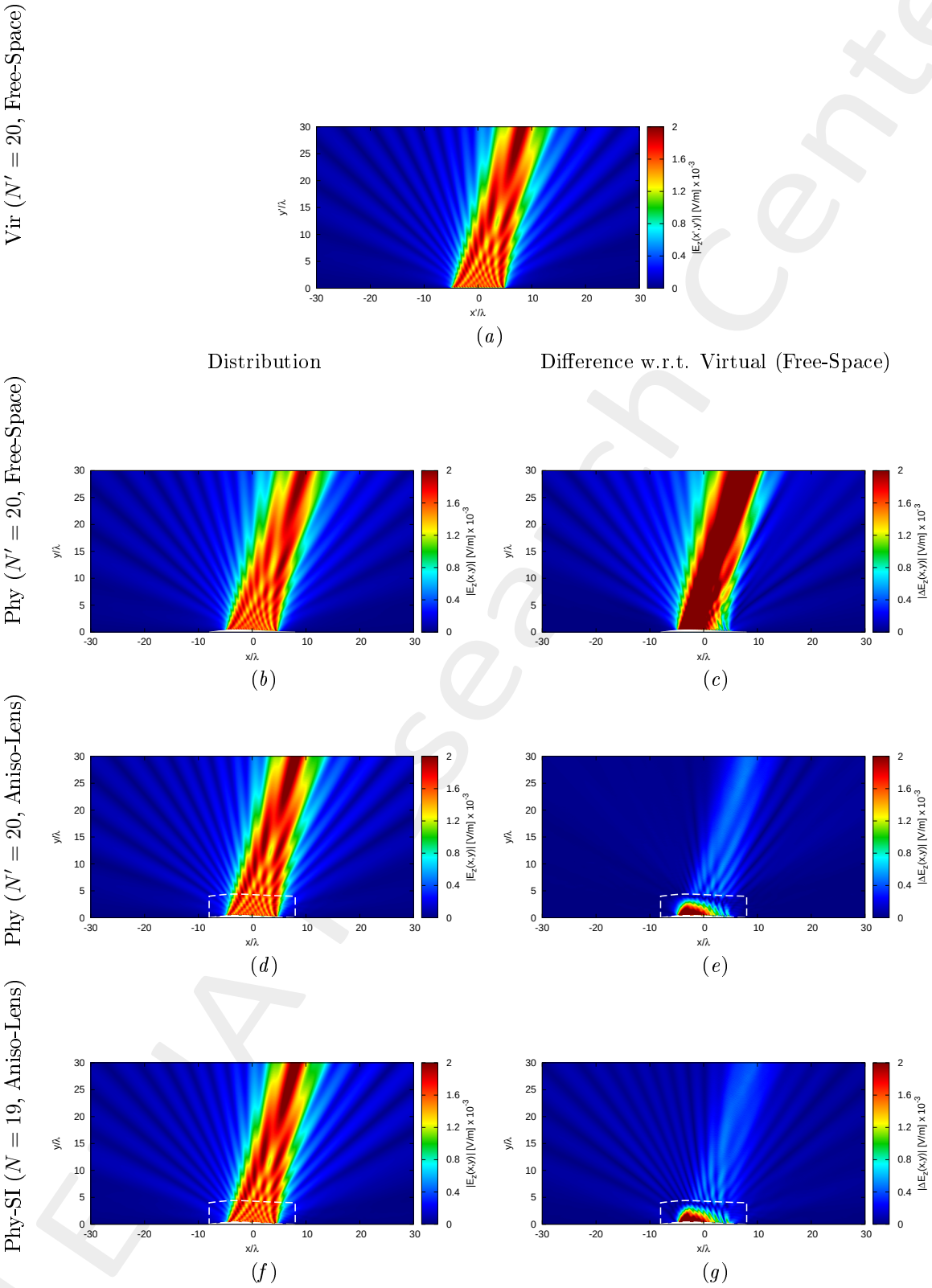

Figure 15: Lens Thickness $s = 4.0$ [λ] - Electric field distributions.

Lens Thickness $s = 2.0$ $[\lambda]$

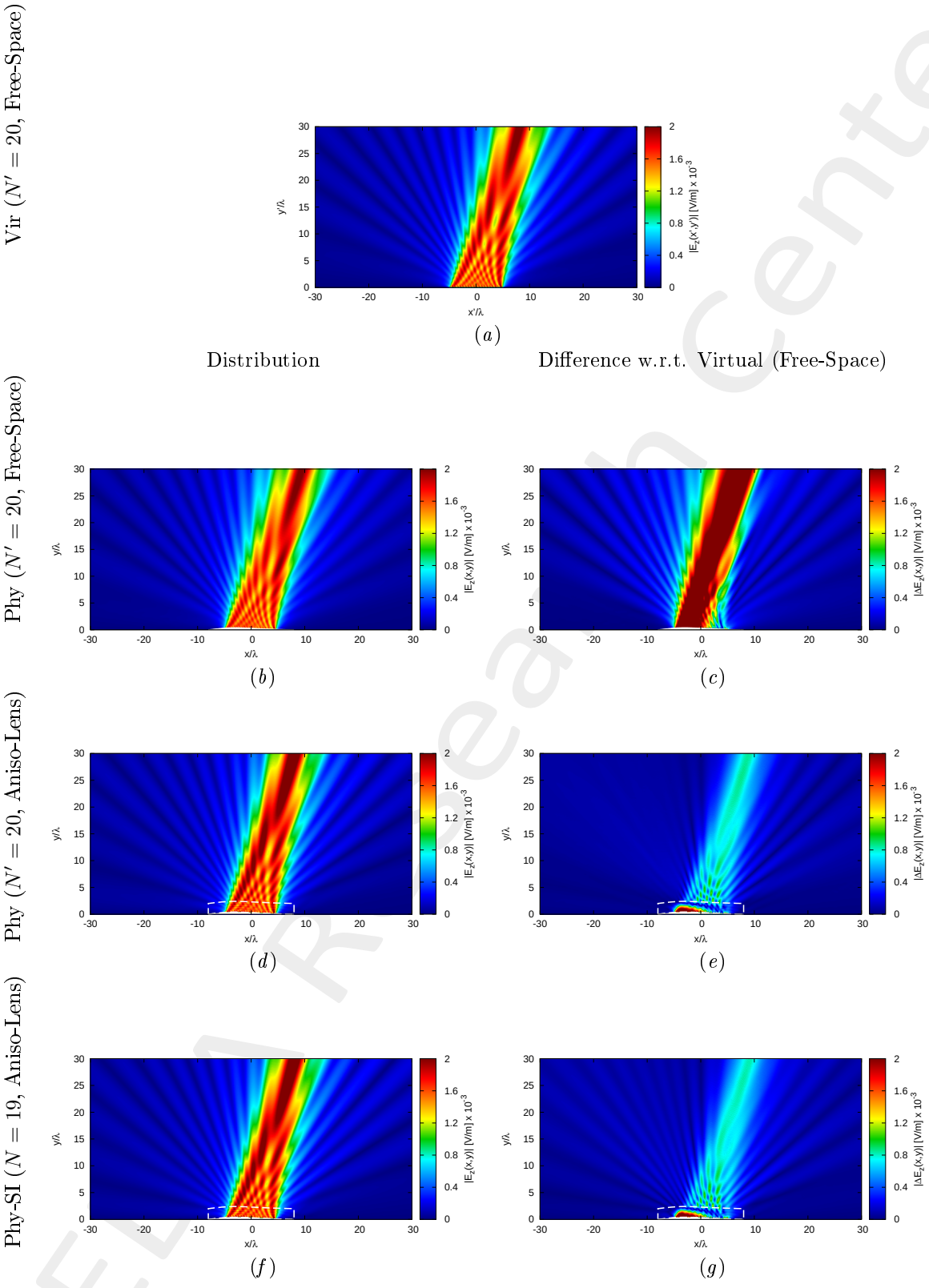

Figure 16: Lens Thickness $s = 2.0$ $[\lambda]$ - Electric field distributions.

1.2.5 Near-Field Distributions (Aniso-Lens, $\phi_s = 105$ [deg])

Lens Thickness $s = 4.0$ [λ]

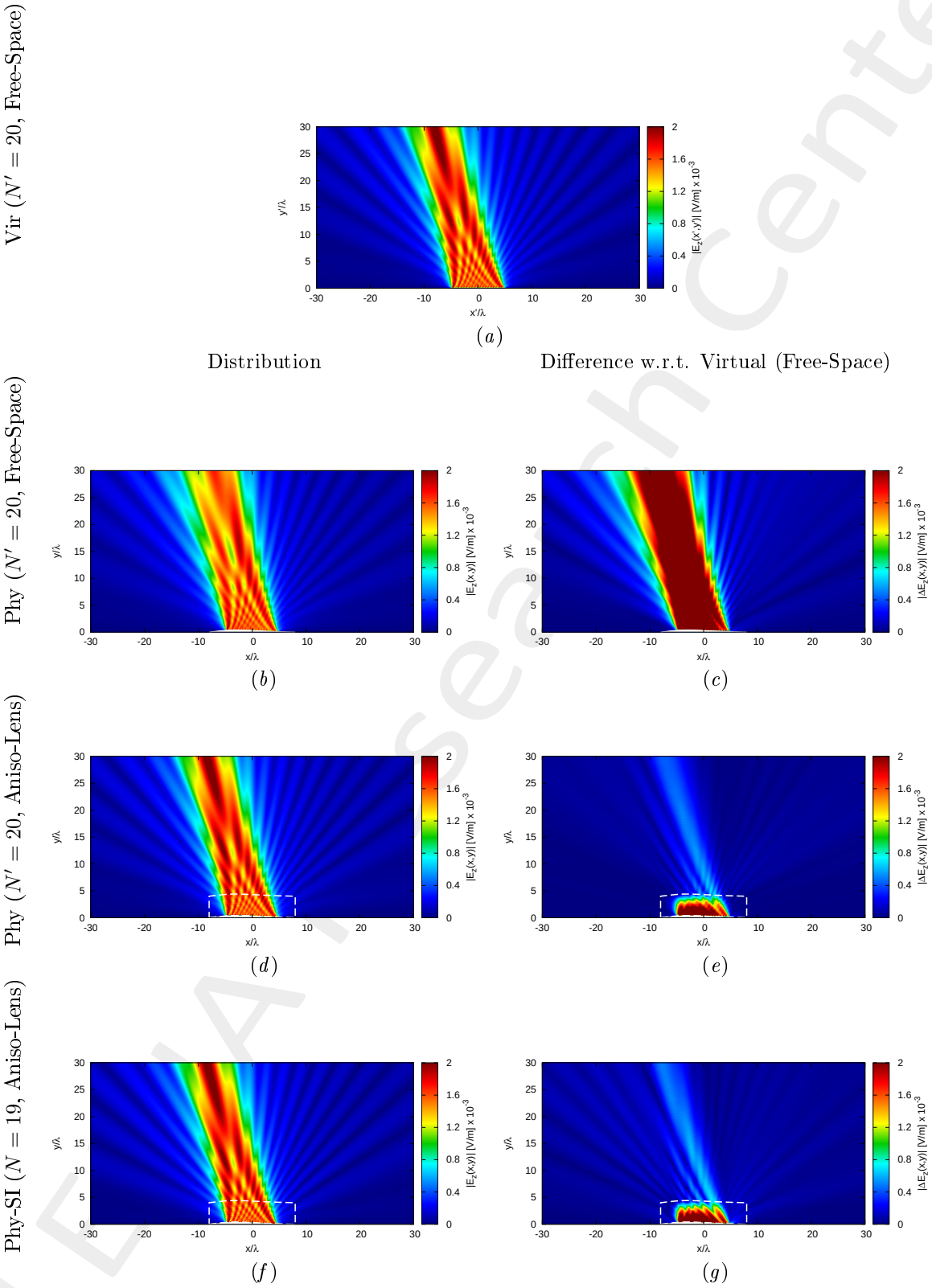

Figure 17: Lens Thickness $s = 4.0$ [λ] - Electric field distributions.

Lens Thickness $s = 2.0$ $[\lambda]$

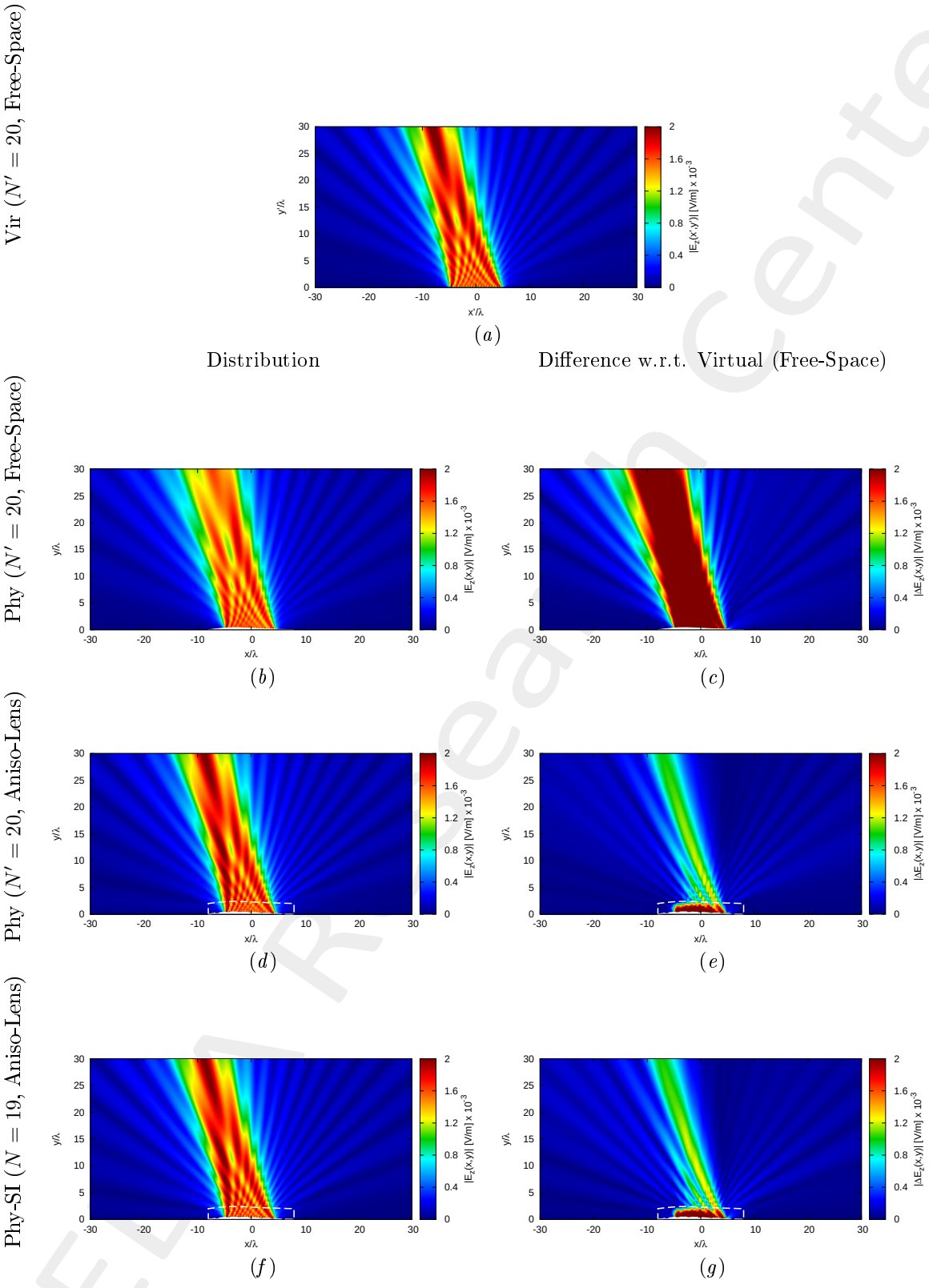

Figure 18: Lens Thickness $s = 2.0$ $[\lambda]$ - Electric field distributions.

1.2.6 Near-Field Distributions (Aniso-Lens, $\phi_s = 60$ [deg])

Lens Thickness $s = 4.0$ [λ]

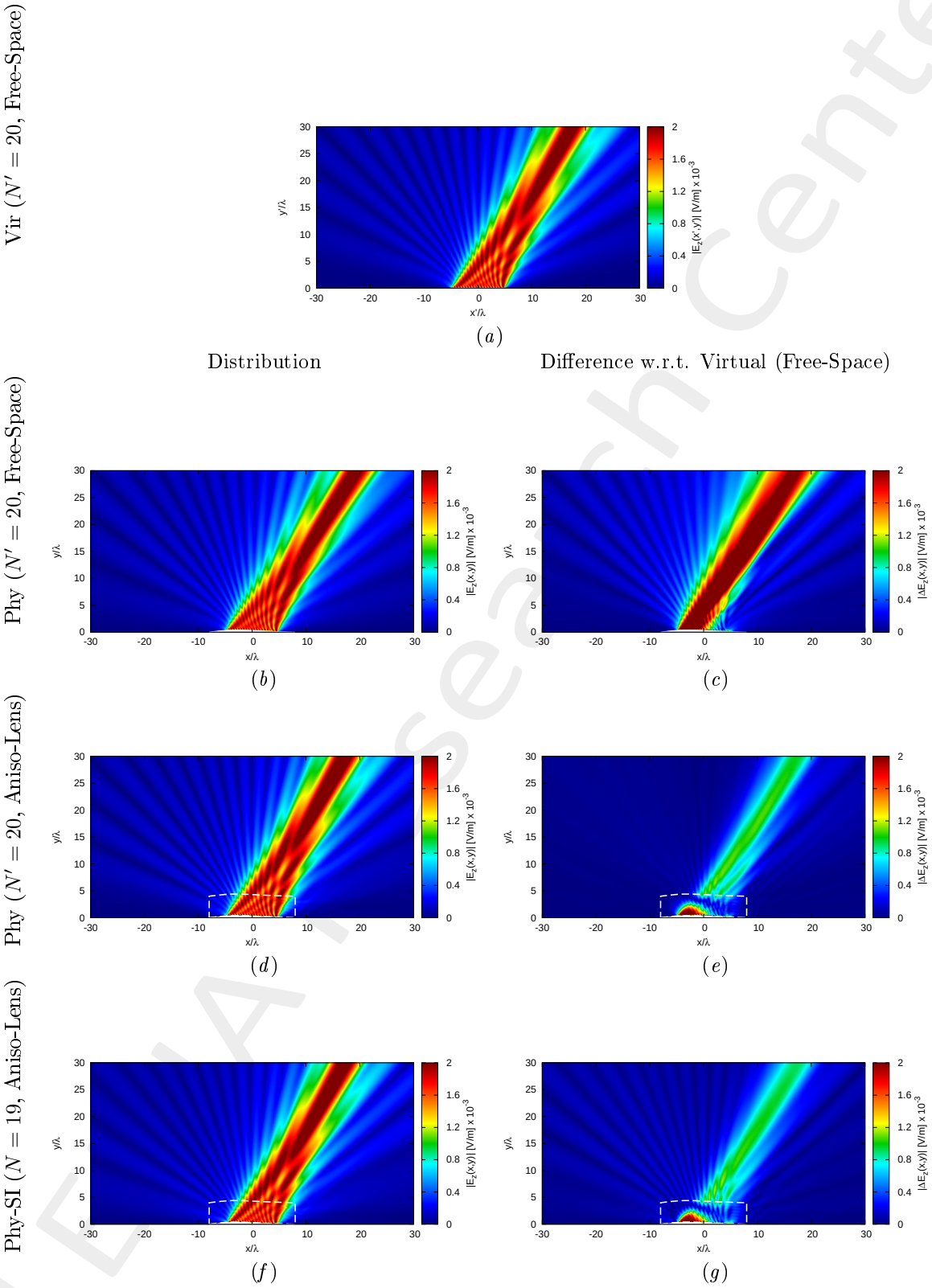

Figure 19: Lens Thickness $s = 4.0$ [λ] - Electric field distributions.

Lens Thickness $s = 2.0$ $[\lambda]$

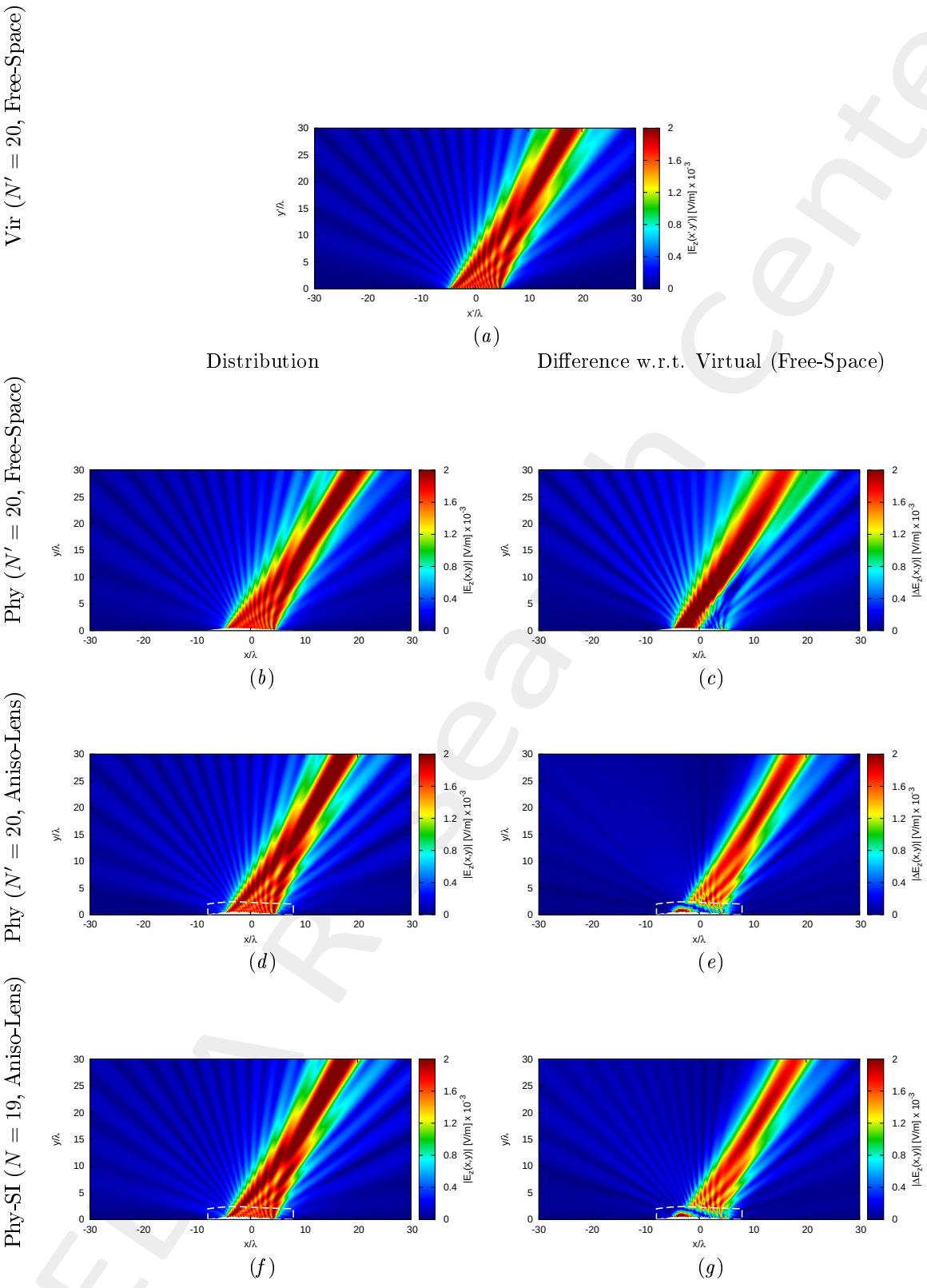

Figure 20: Lens Thickness $s = 2.0$ $[\lambda]$ - Electric field distributions.

1.2.7 Near-Field Distributions (Aniso-Lens, $\phi_s = 120$ [deg])

Lens Thickness $s = 4.0$ [λ]

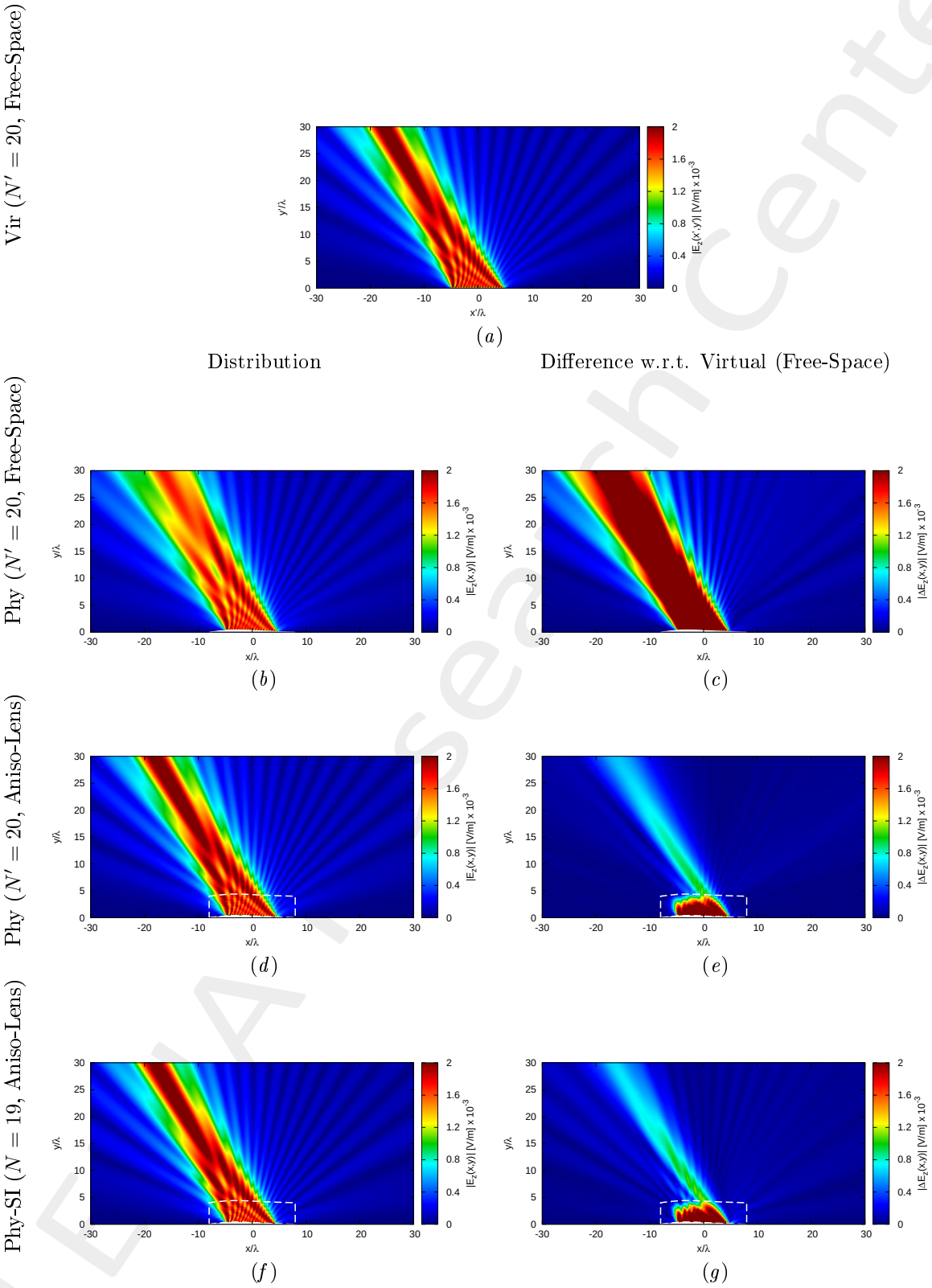

Figure 21: Lens Thickness $s = 4.0$ [λ] - Electric field distributions.

Lens Thickness $s = 2.0$ $[\lambda]$

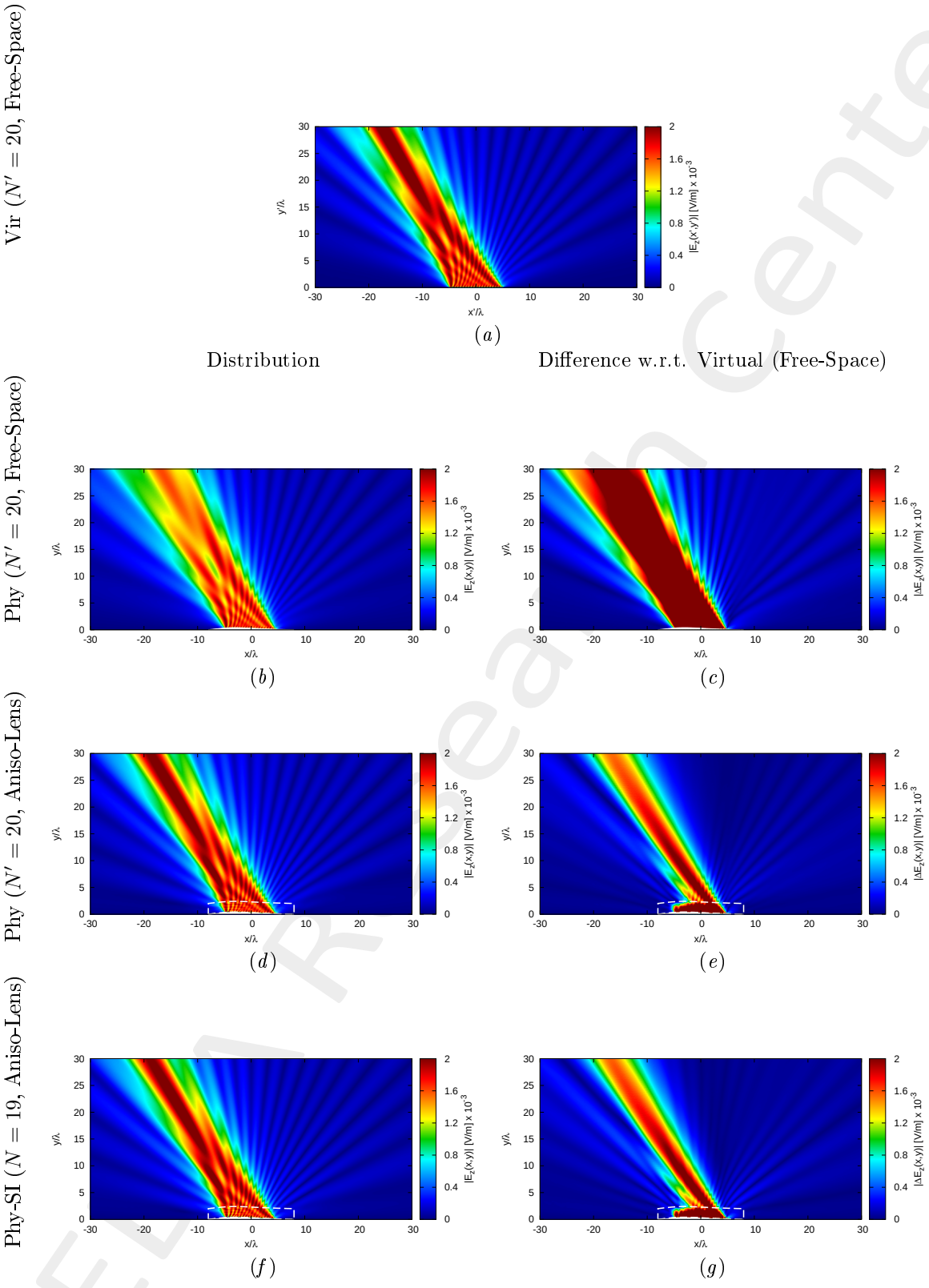

Figure 22: Lens Thickness $s = 2.0$ $[\lambda]$ - Electric field distributions.

1.2.8 Far-Field Patterns (Aniso-Lens)

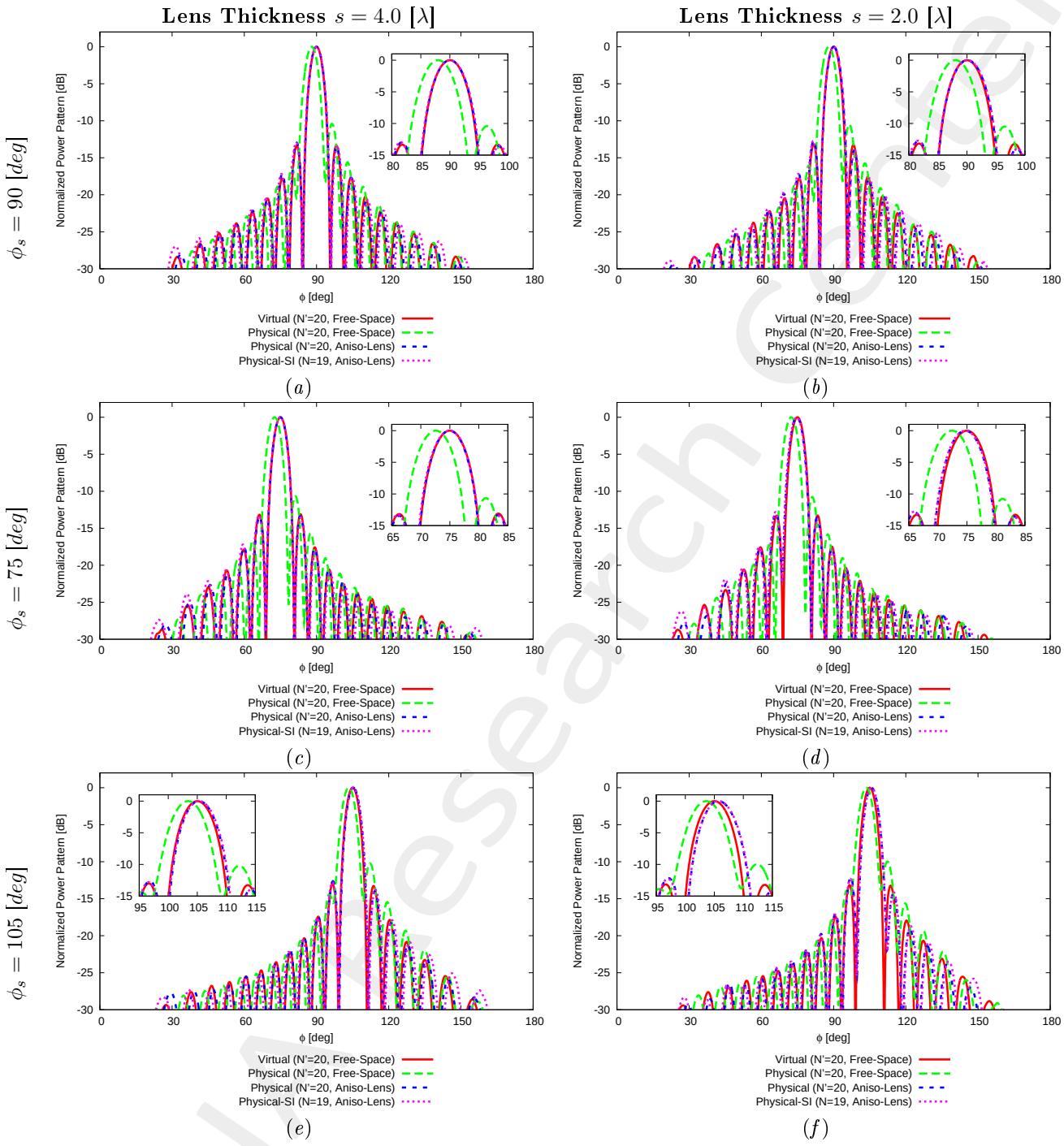

Figure 23: Comparison between the far field patterns.

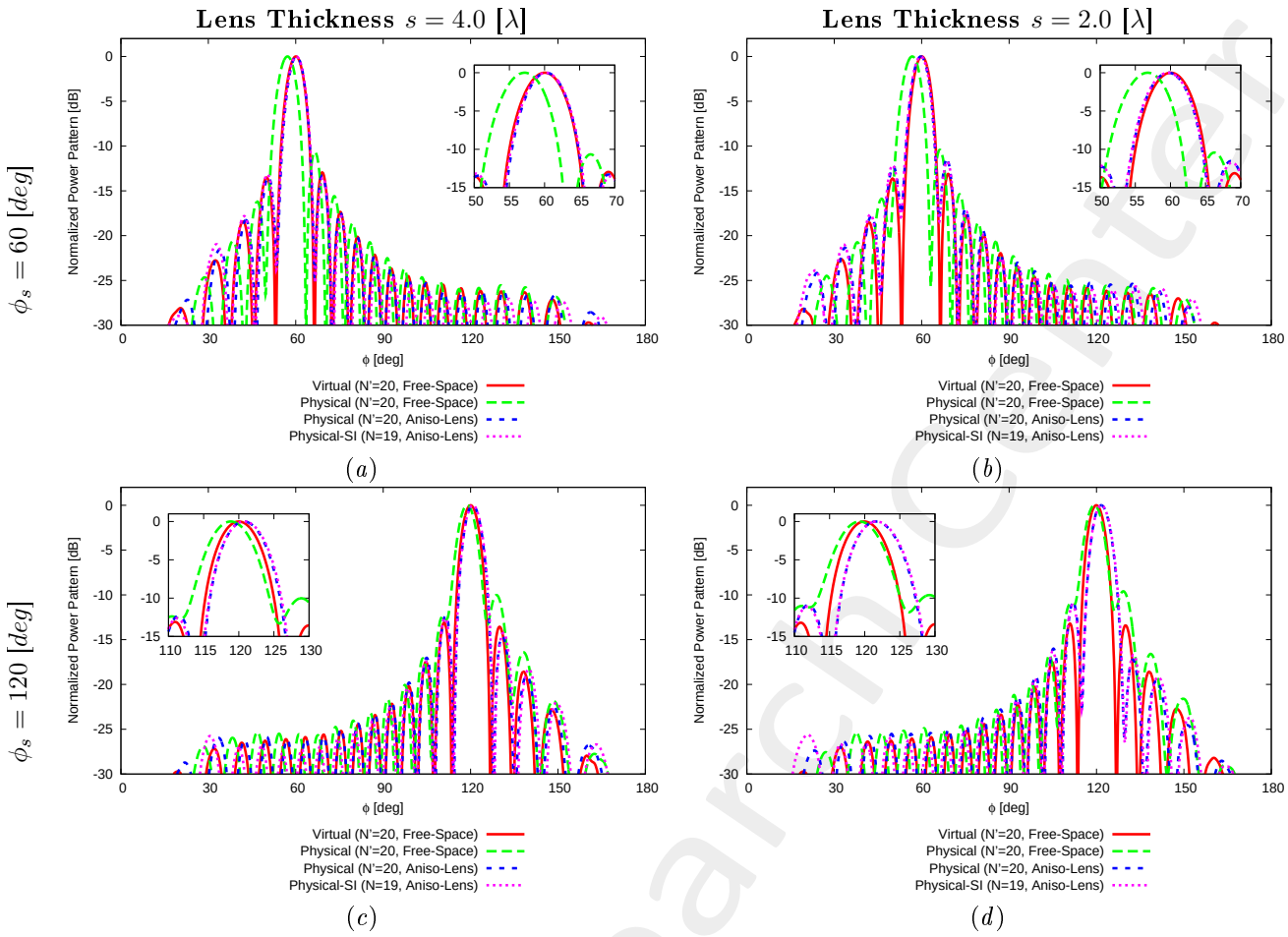

Figure 24: Comparison between the far field patterns.

References

[1] G. Oliveri, G. Gottardi, F. Robol, A. Polo, L. Poli, M. Salucci, M. Chuan, C. Massagrande, P. Vinetti, M. Mattivi, R. Lombardi, and A. Massa, "Co-design of unconventional array architectures and antenna elements for 5G base station," *IEEE Trans. Antennas Propag.*, vol. 65, no. 12, pp. 6752-6767, Dec. 2017.

[2] P. Rocca, G. Oliveri, R. J. Mailloux, and A. Massa, "Unconventional phased array architectures and design methodologies - A review," *Proc. IEEE*, vol. 104, no. 3, pp. 544-560, Mar. 2016.

[3] G. Oliveri, M. Salucci, N. Anselmi and A. Massa, "Multiscale System-by-Design synthesis of printed WAIMs for waveguide array enhancement," *IEEE J. Multiscale Multiphysics Computat. Techn.*, vol. 2, pp. 84-96, 2017.

[4] A. Massa and G. Oliveri, "Metamaterial-by-Design: Theory, methods, and applications to communications and sensing - Editorial," *EPJ Applied Metamaterials*, vol. 3, no. E1, pp. 1-3, 2016.

[5] L. Poli, G. Oliveri, P. Rocca, M. Salucci, and A. Massa, "Long-Distance WPT Unconventional Arrays Synthesis," *J. Electromagnet. Waves Appl.*, vol. 31, no. 14, pp. 1399-1420, Jul. 2017.

[6] G. Oliveri, F. Viani, N. Anselmi, and A. Massa, "Synthesis of multi-layer WAIM coatings for planar phased arrays within the system-by-design framework," *IEEE Trans. Antennas Propag.*, vol. 63, no. 6, pp. 2482-2496, Jun. 2015.

[7] G. Oliveri, L. Tenuti, E. Bekele, M. Carlin, and A. Massa, "An SbD-QCTO approach to the synthesis of isotropic metamaterial lenses," *IEEE Antennas Wireless Propag. Lett.*, vol. 13, pp. 1783-1786, 2014.

[8] G. Oliveri, D. H. Werner, and A. Massa, "Reconfigurable electromagnetics through metamaterials - A review" *Proc. IEEE*, vol. 103, no. 7, pp. 1034-1056, Jul. 2015.

[9] G. Oliveri, E. T. Bekele, M. Salucci, and A. Massa, "Transformation electromagnetics miniaturization of sectoral and conical horn antennas," *IEEE Trans. Antennas Propag.*, vol. 64, no. 4, pp. 1508-1513, Apr. 2016.

[10] G. Oliveri, E. T. Bekele, M. Salucci, and A. Massa, "Array miniaturization through QCTO-SI metamaterial radomes," *IEEE Trans. Antennas Propag.*, vol. 63, no. 8, pp. 3465-3476, Aug. 2015.

[11] G. Oliveri, E. T. Bekele, D. H. Werner, J. P. Turpin, and A. Massa, "Generalized QCTO for metamaterial-lens-coated conformal arrays," *IEEE Trans. Antennas Propag.*, vol. 62, no. 8, pp 4089-4095, Aug. 2014.

[12] G. Oliveri, E. Bekele, M. Carlin, L. Tenuti, J. Turpin, D. H. Werner, and A. Massa, "Extended QCTO for innovative antenna system designs," IEEE Antenna Conference on Antenna Measurements and Applications (CAMA 2014), pp. 1-3, Nov. 16-19, 2014.

[13] G. Oliveri, P. Rocca, M. Salucci, E. T. Bekele, D. H. Werner, and A. Massa, "Design and synthesis of innovative metamaterial-enhanced arrays," IEEE International Symposium on Antennas Propag. (APS/URSI 2013), Orlando, Florida, USA, pp. 972 - 973, Jul. 7-12, 2013.

[14] G. Oliveri, "Improving the reliability of frequency domain simulators in the presence of homogeneous metamaterials - A preliminary numerical assessment," *Progress In Electromagnetics Research*, vol. 122, pp. 497-518, 2012.

[15] M. Salucci, G. Oliveri, N. Anselmi, G. Gottardi, and A. Massa, "Performance enhancement of linear active electronically-scanned arrays by means of MbD-synthesized metalenses," *J. Electromagnet. Waves Appl.*, vol. 32, no. 8, pp. 927-955, 2018.

[16] M. Salucci, G. Oliveri, N. Anselmi, and A. Massa, "Material-by-design synthesis of conformal miniaturized linear phased arrays," *IEEE Access* (doi: 10.1109/ACCESS.2018.2833199).